Structural Engineering and Mechanics, Vol. 7, No. 1 (1999) 111-126
DOI: http://dx.doi.org/10.12989/sem.1999.7.1.111

Sensitivity and optimisation procedures for truss structures under large displacement

A.S. Bothma† and J. Ronda‡

Department of Mathematics and Applied Mathematics, University of Cape Town, South Africa

M. Kleiber‡†

Institute of Fundamental Technological Research, Polish Academy of Sciences, Poland

Abstract. The work presented here focuses on the development of suitable discretised formulations, for large-displacement shape and non-shape design sensitivity analysis (DSA), which enable the straightforward incorporation of structural optimisation into established finite element analysis (FEA) codes. For the generalised displacement-based functional the design sensitivity vector has been expressed in terms of displacement sensitivity. The Total Lagrangian formulation is utilised for modelling of large deformation of truss structures. The variational formulation of the sensitivity analysis procedure is discretised by using "pseudo"- finite elements. Results are presented for the sensitivity analysis and optimisation of standard truss structures. For the purposes of this work, the analysis and optimisation procedures outlined below are incorporated into the FEA code ABAQUS.

Key words: structural optimisation; design sensitivity analysis; finite element method.

1. Introduction

The purpose of structural optimisation is to minimise a generalised cost functional

$$f \equiv f(\boldsymbol{u}, \boldsymbol{b}) \equiv f(\boldsymbol{u}(\boldsymbol{b}), \boldsymbol{b})$$

for *shape* or *non-shape* design parameters $\boldsymbol{b}$, subject to a set of generalised equality and inequality constraints

$$g_i \equiv g_i(\boldsymbol{u}, \boldsymbol{b}) \equiv g_i(\boldsymbol{u}(\boldsymbol{b}), \boldsymbol{b})$$

where u is the generalized displacement.

Commonly f represents the volume of material employed in a structure, or the financial cost proportional to the volume of material, whereas the constraints g_i generally reflect displacement, strain or stress limits imposed on the structural behaviour.

† M. Sc., Private Bag, Rondebosch 7700, South Africa
‡ D. Sc., Private Bag, Rondebosch 7700, South Africa
‡† Professor, Polish Academy of Science, Swietokyska 21, 00-49 Warsaw, Poland

The object of DSA is to obtain a vector, $\nabla_b \Psi \equiv \frac{d\Psi}{db}$, which expresses the perturbation of a functional Ψ subject to variation of the design parameters $\boldsymbol{b}$. These sensitivities are crucial in implementing structural optimisation; i.e., DSA is utilised to evaluate

$$\nabla_b f, \nabla_b g_i \qquad i \in I_\varepsilon,\ \varepsilon = \{\text{active constraints}\}$$

The design parameters $\boldsymbol{b}$ for problems in engineering mechanics fall broadly into four categories:[1] (Mróz 1994)

1. parameters which influence the elasticity (or elastic-predictor) matrix (i.e., the material model),
2. shape or configuration variables (i.e., the geometric design of a structure),
3. support and loading conditions,
4. topological support parameters, e.g., number of joints, elements or connections.

Recent increases in computing power have enabled the application of sophisticated computational optimisation procedures to a range of engineering problems in design and manufacturing. Theoretical advances in structural optimisation and sensitivity analysis now allow for the investigation of problems variously involving time- and path-dependent material behaviour, dynamic response characteristics, kinematic nonlinearity and higher-order element formulations (Tsay and Arora 1990, Kleiber *et al.* 1994, and Kleiber 1993). The increasing complexity of such sensitivity and optimisation procedures translates directly into increased design effort. Much time and effort can be saved by incorporating optimisation procedures directly into an established FEA code, thereby taking advantage of the facilities already available in the particular code (Arora and Cardosa 1989, and Haririan *et al.* 1987).

Incorporating design optimisation in an established finite element analysis (FEA) code, care has to be taken to ensure that the sensitivity analysis procedures are formulated and discretised in a FEA compatible manner: the ensuing sections elaborate on the development and implementation of such 'pseudo'-FE discretisations for the *shape* or *non-shape* sensitivity analysis of displacement- and stress-based functionals.

The total Lagrangian (TL) kinematic formulation is utilised to allow for the accurate modelling of large displacement behaviour during both the structural and sensitivity analysis phases. The Direct Differentiation Method (DDM) was selected for the purposes of performing DSA. The DDM was chosen due primarily to its straightforward formulation and comparatively better behaviour for complex material models. The general robustness and efficiency of the recursive quadratic programming (RQP) method motivated the preference of the PLBA approach as an optimisation procedure (Belegundu and Arora 1985, Lim and Arora 1986, Thanedar *et al.* 1986). Results are generated for two standard benchmark truss structures, respectively illustrated in Fig. 2 and Fig. 5.

2. Sensitivity analysis formulation

The design sensitivity vector $\nabla_b \Psi$ for the generalised displacement-based functional

$$\Psi \equiv \Psi(\boldsymbol{u}, \boldsymbol{b}) \equiv \Psi(\boldsymbol{u}(\boldsymbol{b}), \boldsymbol{b}) \tag{1}$$

[1] In this work only category **1** and **2** parameter sensitivities are investigated, generally referred to as *non-shape* and *shape* sensitivity, respectively. Fig. 6 provides a graphical definition of the design parameters emplyoed in one of the applications considered here.

is expressed in terms of displacement sensitivity, $\frac{du}{db}$, as

$$\nabla_b \Psi = \frac{d\Psi}{db} = \frac{\partial \Psi}{\partial u}\frac{du}{db} + \frac{\partial \Psi}{\partial b} \tag{2}$$

where $\frac{\partial \Psi}{\partial u}$, as well as the *explicit* dependency of Ψ on b, $\frac{\partial \Psi}{\partial b}$, are analytically derived.

The DDM is used to evaluate $\frac{du}{db}$:

Representing the state of equilibrium of a system, at time $t+\Delta t$, by

$${}^{t+\Delta t}F(u, b) = 0$$

the DDM proceeds by separating the design sensitivity operator $\bar{\delta} \equiv \nabla_b$ into *implicit* and *explicit* parts:

$$\bar{\delta}({}^{t+\Delta t}F) = (\tilde{\delta} + \bar{\bar{\delta}})\,{}^{t+\Delta t}F = 0 \tag{3}$$

where, from (Tsay and Arora 1990),

$$\tilde{\delta} \equiv \frac{du}{db}\frac{\partial}{\partial u}, \qquad \bar{\bar{\delta}} \equiv \frac{\partial}{\partial b}$$

For a mechanical system

$${}^{t+\Delta t}F(u, b) \equiv Q(u, b) - {}^{t+\Delta t}\Re = 0 \tag{4}$$

with

$$Q(u, b) = {}^{t+\Delta t}_{0}Q \equiv \int_{{}^{0}V} {}^{t+\Delta t}_{0}S_{ij}\ {}^{t+\Delta t}_{0}\delta\varepsilon_{ij}\ {}^{0}dV \qquad \text{for } TL$$

$$Q(u, b) = {}^{t+\Delta t}Q \equiv \int_{{}^{t+\Delta t}V} {}^{t+\Delta t}\tau_{ij}\ {}^{t+\Delta t}\delta e_{ij}\ {}^{t+\Delta t}dV \qquad \text{for } UL$$

and[2]

$${}^{t+\Delta t}\Re = \int_{{}^{0}V} {}^{t+\Delta t}_{0}\rho\ {}^{t+\Delta t}_{0}\delta u^{\top} \cdot {}^{t+\Delta t}_{0}f\ {}^{0}dV + \int_{{}^{0}T_t} {}^{t+\Delta t}_{0}\delta u^{T} \cdot {}^{t+\Delta t}_{0}t\ {}^{0}dT_t$$

Considering only the *TL* formulation, Eq. (3) is restated as

$$\tilde{\delta}\left(\int_{{}^{0}V} {}^{t+\Delta t}_{0}S\ {}^{t+\Delta t}_{0}\delta\varepsilon\ {}^{0}dV - {}^{t+\Delta t}\Re\right) + \bar{\bar{\delta}}\left(\int_{{}^{0}V} {}^{t+\Delta t}_{0}S\ {}^{t+\Delta t}_{0}\delta\varepsilon\ {}^{0}dV - {}^{t+\Delta t}\Re\right) = 0 \tag{5}$$

by substituting Eq. (4).

The expression in Eq. (5) is reformulated in the 'natural' frame[3] C_r and expanded as

$$\left\{ \int_{{}^{r}V} \tilde{\delta}({}^{t+\Delta t}_{0}\delta\varepsilon^{\top} \cdot {}^{t+\Delta t}_{0}S\ J)\,{}^{r}dV + \int_{{}^{r}V} \bar{\bar{\delta}}({}^{t+\Delta t}_{0}\delta\varepsilon^{\top} \cdot {}^{t+\Delta t}_{0}S\ J)\,{}^{r}dV \right\}$$

[2] Assuming deformation independence of the traction load and material incompressibility, the expression ${}^{t+\Delta t}R$ is utilised for both *TL* and *UL* kinematic formulations.

[3] Fig. 1 details the isoparametric mapping from the 'parent' frame C_r to the 'global' frame C_0. C_0' refers to an intermediate 'local' frame.

$$-\left\{\int_{r_V} \tilde{\delta}({}_0^{t+\Delta t}\rho\, {}_0^{t+\Delta t}\delta \boldsymbol{u}^{\top} \cdot {}_0^{t+\Delta t}\boldsymbol{f}\, J)\, {}^{r}dV + \int_{r_V} \bar{\bar{\delta}}({}_0^{t+\Delta t}\rho\, {}_0^{t+\Delta t}\delta \boldsymbol{u}^{\top} \cdot {}_0^{t+\Delta t}\boldsymbol{f}\, J)\, {}^{r}dV\right\}$$
$$-\left\{\int_{r_{\Gamma_t}} \tilde{\delta}({}_0^{t+\Delta t}\delta \boldsymbol{u}^{\top} \cdot {}_0^{t+\Delta t}\boldsymbol{t}\, J_{\Gamma})\, {}^{r}d\Gamma_t + \int_{r_{\Gamma_t}} \bar{\bar{\delta}}({}_0^{t+\Delta t}\delta \boldsymbol{u}^{\top} \cdot {}_0^{t+\Delta t}\boldsymbol{t}\, J_{\Gamma})\, {}^{r}d\Gamma_t\right\} = 0 \tag{6}$$

which is simplified by the introduction of several standard conditions. The slight reduction in generality of the DSA formulation is more than offset by the considerable simplification of Eq. (6):

- Material incompressibility implies

$$^{0}\rho = {}_0^{t}\rho = {}_0^{t+\Delta t}\rho$$

so that effectively

$$\tilde{\delta}({}_0^{t+\Delta t}\rho) = 0$$

- The Jacobian integration factors J and J_{Γ} depend *exclusively* on the isoparametric mapping $C_r \rightarrow C_0$, and as such are deformation independent:

$$\tilde{\delta} J = 0, \quad \tilde{\delta} J_{\Gamma} = 0$$

- ${}_0^{t+\Delta t}\delta \boldsymbol{u}$ is arbitrary and, therefore, design parameter independent:

$$\bar{\delta}({}_0^{t+\Delta t}\delta \boldsymbol{u}) = \tilde{\delta}({}_0^{t+\Delta t}\delta \boldsymbol{u}) + \bar{\bar{\delta}}({}_0^{t+\Delta t}\delta \boldsymbol{u}) = 0$$

- Assuming 'non-follower' forces, i.e., the traction ${}_0^{t+\Delta t}\boldsymbol{t}$ and body force ${}_0^{t+\Delta t}\boldsymbol{f}$ are not deformation dependent:

$$\tilde{\delta}({}_0^{t+\Delta t}\boldsymbol{t}) = 0, \quad \tilde{\delta}({}_0^{t+\Delta t}\boldsymbol{f}) = 0$$

Imposing the conditions above, Eq. (6) reduces to

$$\int_{r_V} \tilde{\delta}({}_0^{t+\Delta t}\delta \boldsymbol{\varepsilon}^{\top} \cdot {}_0^{t+\Delta t}\boldsymbol{S})\, J\, {}^{r}dV + \int_{r_V} \bar{\bar{\delta}}({}_0^{t+\Delta t}\delta \boldsymbol{\varepsilon}^{\top} \cdot {}_0^{t+\Delta t}\boldsymbol{S}\, J)\, {}^{r}dV$$
$$-\int_{r_V} \bar{\bar{\delta}}({}_0^{t+\Delta t}\rho\, {}_0^{t+\Delta t}\delta \boldsymbol{u}^{\top} \cdot {}_0^{t+\Delta t}\boldsymbol{f}\, J)\, {}^{r}dV - \int_{r_{\Gamma_t}} \bar{\bar{\delta}}({}_0^{t+\Delta t}\delta \boldsymbol{u}^{\top} \cdot {}_0^{t+\Delta t}\boldsymbol{t}\, J_{\Gamma})\, {}^{r}d\Gamma_t = 0 \tag{7}$$

The following specific assumptions are introduced in order to simplify Eq. (7) for the particular applications considered here:

- Body force is negligible compared to traction, thus

$${}_0^{t+\Delta t}\boldsymbol{f} \rightarrow 0$$

- Traction force ${}_0^{t+\Delta t}\boldsymbol{t}$ has no *shape* or *non-shape* design parameter dependence

$$\bar{\bar{\delta}}({}_0^{t+\Delta t}\boldsymbol{t}) = 0$$

- Traction ${}_0^{t+\Delta t}\boldsymbol{t}$ is a concentrated nodal force, so that

$$\int_{r_V} \bar{\bar{\delta}}({}_0^{t+\Delta t}\delta \boldsymbol{u}^{\top} \cdot {}_0^{t+\Delta t}\boldsymbol{t}\, J_{\Gamma})\, {}^{r}d\Gamma_t$$
$$= [\bar{\bar{\delta}}({}_0^{t+\Delta t}\delta \boldsymbol{u}^{\top} \cdot {}_0^{t+\Delta t}\boldsymbol{t})]_{node=1} + [\bar{\bar{\delta}}({}_0^{t+\Delta t}\delta \boldsymbol{u}^{\top} \cdot {}_0^{t+\Delta t}\boldsymbol{t})]_{node=2} = 0$$

Introducing these further assumptions into Eq. (7), the variational form of the DSA formulation

may then simply be stated as

$$\int_{r_V} \tilde{\delta}({}_0^{t+\Delta t}\delta\varepsilon^{\top} \cdot {}_0^{t+\Delta t}\boldsymbol{S})\, J\, {}^{r}dV + \int_{r_V} \tilde{\bar{\delta}}({}_0^{t+\Delta t}\delta\varepsilon^{\top} \cdot {}_0^{t+\Delta t}\boldsymbol{S}\, J)\, {}^{r}dV = 0 \tag{8}$$

which applies generally to problems involving *shape* or *non-shape* design parameters, subject to the constraints and assumptions imposed above.

3. Discretising the DSA formulation

As a precondition to implementing DSA in ABAQUS, the variational formulation for the sensitivity analysis procedure Eq. (8) is discretised in a 'pseudo'-finite element fashion. For *shape* and *non-shape* DSA, the discretised variational formulation is expressed in terms of a 'pseudo'-stiffness $\boldsymbol{K}'$, 'pseudo'-load $\boldsymbol{R}'$ and 'pseudo'-displacement $\nabla_b\, {}_0^{t+\Delta t}\boldsymbol{u}$:

$$\boldsymbol{K}' \cdot \nabla_b\, {}_0^{t+\Delta t}\boldsymbol{u} = R'$$

A kinematically nonlinear truss/bar element discretisation is utilised throughout.

3.1. Non-shape DSA

Adopting truss cross-sectional area $b_i \equiv A$ as a *non-shape* design parameter, as illustrated in Fig. 6, the 'pseudo'-stiffness takes on the form:

$$\boldsymbol{K}' = {}^{0}\boldsymbol{T}^{\top} \cdot \boldsymbol{M} \cdot {}^{0}\boldsymbol{T} \tag{9}$$

where

$$\boldsymbol{M} = (E\ {}^{0}L\ {}^{0}A)\,[{}^{0}\tilde{\tilde{\aleph}}^{\top} \cdot {}^{0}\boldsymbol{T} \cdot {}_0^{t+\Delta t}\boldsymbol{u} \cdot {}^{0}\tilde{\aleph} + {}^{0}\tilde{\aleph} \cdot {}_0^{t+\Delta t}\boldsymbol{u}^{\top} \cdot {}^{0}\boldsymbol{T}^{\top} \cdot (\tfrac{1}{2})\, {}^{0}\aleph + {}^{0}\tilde{\aleph} \cdot {}^{0}\tilde{\tilde{\aleph}}^{\top}]$$

for

$${}^{0}L \equiv \text{truss length}$$
$$E \equiv \text{Young's modulus}$$
$${}^{0}\boldsymbol{T}^{\top} = [{}_{0'}^{0}x_{i,j}] \equiv \left[\frac{\partial\, {}^{0}x_i}{\partial\, {}^{0}x_j{}'}\right]$$

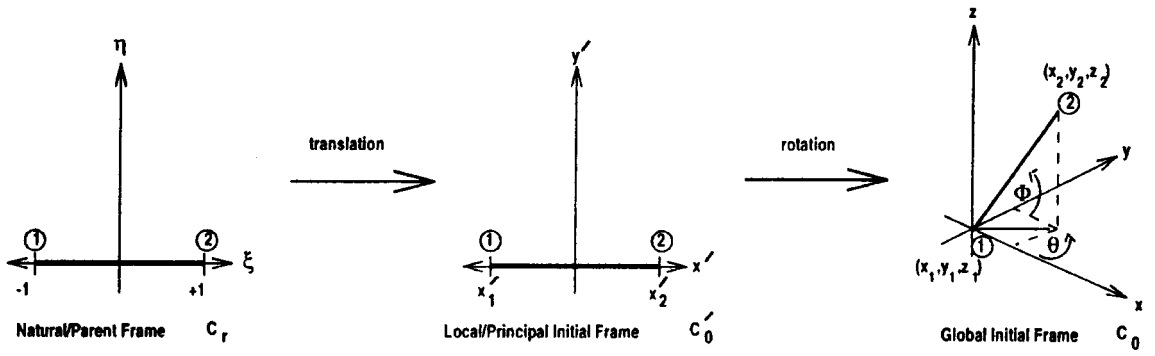

Fig. 1 The isoparametric mapping

$$
{}^0\boldsymbol{N}^{\top}_{x,x} = \frac{1}{{}^0L}[-1\ 0\ 0\ 1\ 0\ 0]
$$

$$
{}^0\boldsymbol{N}^{\top}_{y,x} = \frac{1}{{}^0L}[0\ -1\ 0\ 0\ 1\ 0]
$$

$$
{}^0\boldsymbol{N}^{\top}_{z,x} = \frac{1}{{}^0L}[0\ 0\ -1\ 0\ 0\ 1]
$$

$$
{}^0\boldsymbol{\aleph} = {}^0\boldsymbol{N}_{x,x} \otimes {}^0\boldsymbol{N}^{\top}_{x,x} + {}^0\boldsymbol{N}_{y,x} \otimes {}^0\boldsymbol{N}^{\top}_{y,x} + {}^0\boldsymbol{N}_{z,x} \otimes {}^0\boldsymbol{N}^{\top}_{z,x}
$$

$$
{}^0\tilde{\boldsymbol{\aleph}} = {}^0\boldsymbol{N}_{x,x} + {}^0\boldsymbol{\aleph} \cdot {}^0\boldsymbol{T} \cdot {}^{t+\Delta t}_{0}\boldsymbol{u}
$$

$$
{}^0\tilde{\tilde{\boldsymbol{\aleph}}} = {}^0\boldsymbol{N}_{x,x} + \frac{1}{2}\,{}^0\boldsymbol{\aleph} \cdot {}^0\boldsymbol{T} \cdot {}^{t+\Delta t}_{0}\boldsymbol{u}
$$

The 'pseudo'-load is expressed as

$$
\boldsymbol{R}' = -[{}^0\boldsymbol{T}^{\top} \cdot \overline{\boldsymbol{\mathcal{K}}} \cdot {}^0\boldsymbol{T} \cdot {}^{t+\Delta t}_{0}\boldsymbol{u}]
$$

where

$$
\overline{\boldsymbol{\mathcal{K}}} = \nabla_{0_A} \boldsymbol{\mathcal{K}} = ({}^0L\ E)\,{}^0\tilde{\boldsymbol{\aleph}} \cdot {}^0\tilde{\tilde{\boldsymbol{\aleph}}}^{\top}
$$

3.2. Shape DSA

Selecting the base area index h of the pylon, illustrated in Fig. 6, as a *shape* design parameter, the 'pseudo'-stiffness $\boldsymbol{K}'$ is unaffected and remains as defined in Eq. (9). The 'pseudo'-load $\boldsymbol{R}'$ is obtained after substantial analytical manipulation[4]:

$$
\boldsymbol{R}' = -\bar{\bar{\delta}}({}^0\hat{\boldsymbol{T}}^{\top} \cdot \hat{\boldsymbol{\mathcal{K}}} \cdot {}^0\hat{\boldsymbol{T}} \cdot {}^{t+\Delta t}_{0}\boldsymbol{u}) \tag{11}
$$

where

$$
\hat{\boldsymbol{\mathcal{K}}} \equiv ({}^0A\ {}^0\hat{L}\ E)\,{}^0\hat{\tilde{\boldsymbol{\aleph}}} \cdot {}^0\hat{\tilde{\tilde{\boldsymbol{\aleph}}}}^{\top}
$$

$$
{}^0\hat{\tilde{\boldsymbol{\aleph}}} = {}^0\hat{\boldsymbol{N}}_{x,x} + {}^0\hat{\boldsymbol{\aleph}} \cdot {}^0\hat{\boldsymbol{T}} \cdot {}^{t+\Delta t}_{0}\boldsymbol{u},
$$

$$
{}^0\hat{\tilde{\tilde{\boldsymbol{\aleph}}}}^{\top} = {}^0\hat{\boldsymbol{N}}^{\top}_{x,x} + (\tfrac{1}{2})\,{}^{t+\Delta t}_{0}\boldsymbol{u}^{\top} \cdot {}^0\hat{\boldsymbol{T}}^{\top} \cdot {}^0\hat{\boldsymbol{\aleph}}
$$

Evaluating $\bar{\bar{\delta}}(\hat{\boldsymbol{\mathcal{K}}})$ in Eq. (11) produces

$$
\bar{\bar{\delta}}(\hat{\boldsymbol{\mathcal{K}}}) = \bar{\bar{\delta}}({}^0\hat{\tilde{\boldsymbol{\aleph}}}) \cdot ({}^0A\ {}^0\hat{L}\ E)\,{}^0\hat{\tilde{\tilde{\boldsymbol{\aleph}}}} + {}^0\hat{\tilde{\boldsymbol{\aleph}}} \cdot {}^0A\ \delta({}^0L)\,E\,{}^0\hat{\tilde{\tilde{\boldsymbol{\aleph}}}}
$$

$$
+ {}^0\hat{\tilde{\boldsymbol{\aleph}}} \cdot ({}^0A\ {}^0\hat{L}\ E)\,\bar{\bar{\delta}}({}^0\hat{\tilde{\tilde{\boldsymbol{\aleph}}}}),
$$

where

$$
\bar{\bar{\delta}}({}^0\hat{\tilde{\boldsymbol{\aleph}}}) = \left(-\frac{1}{{}^0\hat{L}}\right){}^0\hat{N}_{x,x} \cdot \nabla_b\,{}^0\hat{L} - \left(\frac{2}{{}^0\hat{L}}\right){}^0\hat{\boldsymbol{\aleph}} \cdot \nabla_b\,{}^0\hat{L} \cdot {}^0\hat{\boldsymbol{T}} \cdot {}^{t+\Delta t}_{0}\boldsymbol{u} + {}^0\hat{\boldsymbol{\aleph}} \cdot \bar{\bar{\delta}}({}^0\hat{\boldsymbol{T}}) \cdot {}^{t+\Delta t}_{0}\boldsymbol{u},
$$

[4] $\hat{T}$ indicates a dependency of T on the *shape* design parameter h.

$$\overline{\overline{\delta}}({}^0\hat{\mathbf{R}}^{\top}) = \left(-\frac{1}{{}^0\hat{L}}\right) {}^0\hat{N}_{x,x}^{\top} \cdot \nabla_b \, {}^0\hat{L} + \left(\frac{1}{2}\right) {}_0^{t+\Delta t}\boldsymbol{u}^{\top} \cdot \overline{\overline{\delta}}({}^0\hat{T}^{\top}) \cdot {}^0\hat{\mathbf{R}}$$
$$- \left(\frac{1}{{}^0\hat{L}}\right) {}_0^{t+\Delta t}\boldsymbol{u}^{\top} \cdot {}^0\hat{T}^{\top} \cdot {}^0\hat{\mathbf{R}} \cdot \nabla_b \, {}^0\hat{L}$$

Now, applying the *explicit* sensitivity operator $\overline{\overline{\delta}}(\ldots)$ to the shape parameter dependent *TL* transformation matrix ${}^0\hat{\boldsymbol{T}} \equiv {}^0\hat{\boldsymbol{T}}(\boldsymbol{h})$ in Eq. (10) results in

$$\overline{\overline{\delta}}({}^0\hat{T}) \equiv \nabla_b \, {}^0\hat{\boldsymbol{T}} \equiv \begin{bmatrix} \boldsymbol{\mathcal{T}} & 0_{3\times 3} \\ 0_{3\times 3} & \boldsymbol{\mathcal{T}} \end{bmatrix}$$

where

$$\boldsymbol{\mathcal{T}} = \begin{bmatrix} \{\alpha_c \cos\theta + \cos\phi\beta_c\} & -\{\beta_s\} & -\{\alpha_s \cos\theta + \sin\phi\beta_c\} \\ \{\alpha_c \sin\theta + \cos\phi\beta_s\} & \{\beta_c\} & -\{\alpha_s \sin\theta + \sin\phi\beta_s\} \\ \{\alpha_s\} & 0 & \{\alpha_c\} \end{bmatrix}$$

for

$$\alpha_c = \overline{\overline{\delta}}(\cos\phi), \quad \alpha_s = \overline{\overline{\delta}}(\sin\phi), \quad \beta_c = \overline{\overline{\delta}}(\cos\theta), \quad \beta_s = \overline{\overline{\delta}}(\sin\theta)$$

It remains to derive and calculate the specific form of the expressions

$$\overline{\overline{\delta}}(\sin\theta) = \frac{d\,\sin\theta}{dh}, \quad \overline{\overline{\delta}}(\cos\theta) = \frac{d\,\cos\theta}{dh},$$
$$\overline{\overline{\delta}}(\sin\phi) = \frac{d\,\sin\phi}{dh}, \quad \overline{\overline{\delta}}(\cos\phi) = \frac{d\,\cos\phi}{dh} \tag{12}$$

as well as $\overline{\overline{\delta}}({}^0\hat{L})$, for each element I of the FE discretisation. The expressions in Eq. (12), as well as $\overline{\overline{\delta}}({}^0\hat{L})$, vary with design geometry and are therefore application dependent. For the pylon truss structure in Fig. 5, where the positions of nodes 7-10 are dependent on a *single* shape design parameter h, these expressions take on the form summarised below:

- node: 7 Elements affected: 15, 18, 23

$$\frac{dL}{dh} = \frac{x-y}{L}$$

$$\frac{d\,\sin\theta}{dh} = \frac{-1}{PL} - \left(\frac{y}{PL^2}\right)\left(\frac{x-y}{PL}\right) \qquad \frac{d\cos\theta}{dh} = \frac{1}{PL} - \left(\frac{x}{PL^2}\right)\left(\frac{x-y}{PL}\right)$$

$$\frac{d\,\sin\phi}{dh} = -\left(\frac{z}{L^2}\right)\left(\frac{x-y}{L}\right) \qquad \frac{d\cos\phi}{dh} = \left(\frac{x-y}{PL}\right)\left(\frac{1}{L}\right) - \left(\frac{PL}{L^2}\right)\left(\frac{x-y}{L}\right)$$

- node: 8 Elements affected: 17, 19, 25

$$\frac{dL}{dh} = \frac{-(x+y)}{L}$$

$$\frac{d\sin\theta}{dh} = \frac{-1}{PL} - \left(\frac{y}{PL^2}\right)\left(\frac{-(x+y)}{PL}\right) \qquad \frac{d\cos\theta}{dh} = \frac{-1}{PL} - \left(\frac{x}{PL^2}\right)\left(\frac{-(x+y)}{PL}\right)$$

$$\frac{d\sin\phi}{dh} = -\left(\frac{z}{L^2}\right)\left(\frac{-(x+y)}{L}\right) \qquad \frac{d\cos\phi}{dh} = \left(\frac{-(x+y)}{PL}\right)\left(\frac{1}{L}\right) - \left(\frac{PL}{L^2}\right)\left(\frac{-(x+y)}{L}\right)$$

- node: 9 Elements affected: 16, 21, 24

$$\frac{dL}{dh} = \frac{y-x}{L}$$

$$\frac{d\sin\theta}{dh} = \frac{1}{P\,L} - \left(\frac{y}{PL^2}\right)\left(\frac{y-x}{PL}\right) \qquad \frac{d\cos\theta}{dh} = \frac{-1}{PL} - \left(\frac{x}{PL^2}\right)\left(\frac{y-x}{PL}\right)$$

$$\frac{d\sin\phi}{dh} = -\left(\frac{z}{L^2}\right)\left(\frac{y-x}{L}\right) \qquad \frac{d\cos\phi}{dh} = \left(\frac{y-x}{PL}\right)\left(\frac{1}{L}\right) - \left(\frac{PL}{L^2}\right)\left(\frac{y-x}{L}\right)$$

- node: 10 Elements affected: 14, 20, 22

$$\frac{dL}{dh} = \frac{x+y}{L}$$

$$\frac{d\sin\theta}{dh} = \frac{1}{PL} - \left(\frac{y}{PL^2}\right)\left(\frac{x+y}{PL}\right) \qquad \frac{d\cos\theta}{dh} = \frac{1}{PL} - \left(\frac{x}{PL^2}\right)\left(\frac{x+y}{PL}\right)$$

$$\frac{d\sin\phi}{dh} = -\left(\frac{z}{L^2}\right)\left(\frac{x+y}{L}\right) \qquad \frac{d\sin\phi}{dh} = \left(\frac{x+y}{PL}\right)\left(\frac{1}{L}\right) - \left(\frac{PL}{L^2}\right)\left(\frac{x+y}{L}\right)$$

where the symbols x, y and z all pertain to node 1 in the parent frame, i.e., $x \equiv x_{(1)}$, $y \equiv y_{(1)}$ and $z \equiv z_{(1)}$, and

$$PL = \sqrt{x^2+y^2}, \quad L = \sqrt{x^2+y^2+z^2}$$

3.3. DSA of stress-based response functionals

Implementing the discretised 'pseudo'-FE DSA formulation in ABAQUS is further complicated by generalising the formulation of the response functional Ψ in Eq. (1) to include a stress $\boldsymbol{\tau}$ (or strain $\boldsymbol{\varepsilon}$) dependency:

$$\Psi \equiv \Psi(\boldsymbol{\tau}, \boldsymbol{u}, \boldsymbol{b}) \equiv \Psi(\boldsymbol{\tau}(\boldsymbol{b}), \boldsymbol{u}(\boldsymbol{b}), \boldsymbol{b})$$

The expression in Eq. (2) for the sensitivity vector of the functional Ψ becomes

$$\nabla_{\boldsymbol{b}} \Psi = \frac{\partial \Psi}{\partial \boldsymbol{\tau}} \left(\frac{\partial \boldsymbol{\tau}}{\partial \boldsymbol{u}} \cdot \nabla_{\boldsymbol{b}} \boldsymbol{u} + \frac{\partial \boldsymbol{\tau}}{\partial \boldsymbol{b}} \right) + \frac{\partial \Psi}{\partial \boldsymbol{b}} \tag{13}$$

which reduces to a problem of obtaining the expression $\dfrac{\partial \boldsymbol{\tau}}{\partial \boldsymbol{u}}$, where $\nabla_{\boldsymbol{b}} \boldsymbol{u}$ is evaluated during the sensitivity analysis phase and $\dfrac{\partial \Psi}{\partial \boldsymbol{\tau}}$, $\dfrac{\partial \boldsymbol{\tau}}{\partial \boldsymbol{b}}$ and $\dfrac{\partial \Psi}{\partial \boldsymbol{b}}$ are obtained analytically.

Considering only the *TL* truss element discretisation, the required expression reduces to $\frac{\partial\, {}^{t+\Delta t}\tau_{xx}}{\partial \boldsymbol{u}}$, so that the term $\left(\frac{\partial \boldsymbol{\tau}}{\partial \boldsymbol{u}}\right) \cdot \nabla_b \boldsymbol{u}$ Eq. (13) takes on the form

$$\left(\frac{\partial(\Phi^2)}{\partial \boldsymbol{u}} \cdot \nabla_b \boldsymbol{u}\right) \cdot {}^0\tilde{\tilde{\aleph}}^{\top} \cdot {}^0\boldsymbol{T} \cdot {}^{t+\Delta t}_{0}\boldsymbol{u} + \Phi^2 \left(\frac{\partial\, {}^0\tilde{\tilde{\aleph}}^{\top}}{\partial \boldsymbol{u}} \cdot \nabla_b \boldsymbol{u}\right) \cdot {}^0\boldsymbol{T} \cdot {}^{t+\Delta t}_{0}\boldsymbol{u}$$
$$+ \Phi^2\, {}^0\tilde{\tilde{\aleph}}^{\top} \cdot {}^0\boldsymbol{T} \cdot \left(\frac{\partial\, {}^{t+\Delta t}_{0}\boldsymbol{u}}{\partial \boldsymbol{u}} \cdot \nabla_b \boldsymbol{u}\right)$$
$$= \left(2\Phi \frac{\partial \Phi}{\partial \boldsymbol{u}} \cdot \nabla_b \boldsymbol{u}\right) \cdot {}^0\tilde{\tilde{\aleph}}^{\top} \cdot {}^0\boldsymbol{T} \cdot {}^{t+\Delta t}_{0}\boldsymbol{u} + \left(\frac{1}{2}\right) \Phi^2 (\nabla_b \boldsymbol{u})^{\top} \cdot {}^0\boldsymbol{T}^{\top} \cdot {}^0\aleph \cdot {}^0\boldsymbol{T} \cdot {}^{t+\Delta t}_{0}\boldsymbol{u}$$
$$+ \Phi^2\, {}^0\tilde{\tilde{\aleph}}^{\top} \cdot {}^0\boldsymbol{T} \cdot \nabla_b \boldsymbol{u}$$

where

$$\Phi = \Phi({}^0\phi, {}^{t+\Delta t}\phi, {}^0\theta, {}^{t+\Delta t}\theta)$$
$$= \cos {}^{t+\Delta t}\phi \cos {}^0\phi (\cos {}^{t+\Delta t}\theta \cos {}^0\phi + \sin {}^{t+\Delta t}\theta \sin {}^0\theta)$$

The form of $\frac{\partial \Phi}{\partial \boldsymbol{u}}$ is found from the incremental values $\frac{\partial \cos {}^{t+\Delta t}\phi}{\partial \boldsymbol{u}}$, $\frac{\partial \cos {}^{t+\Delta t}\theta}{\partial \boldsymbol{u}}$, $\frac{\partial \sin {}^{t+\Delta t}\theta}{\partial \boldsymbol{u}}$, $\frac{\partial \cos {}^0\phi}{\partial \boldsymbol{u}}$, $\frac{\partial \cos {}^0\theta}{\partial \boldsymbol{u}}$ and $\frac{\partial \sin {}^0\theta}{\partial \boldsymbol{u}}$. As was the case for *shape* DSA, the formulation of these expressions is specific to the particular application. The particular form of these expressions for the 200-bar truss structure, illustrated in Fig. 2, are presented below: $\frac{\partial}{\partial u_{1x}}$, $\frac{\partial}{\partial u_{2x}}$ and $\frac{\partial}{\partial u_{1y}}$, $\frac{\partial}{\partial u_{2y}}$ represent the *x*- and *y*-direction nodal displacement sensitivities for, respectively, node **1** and **2**, so that:

$$\frac{\partial \cos {}^{t+\Delta t}\theta}{\partial u_{1x}} = \frac{1}{\gamma}\left(\frac{\alpha^2}{\gamma^2} - 1\right) \qquad \frac{\partial \sin {}^{t+\Delta t}\theta}{\partial u_{1x}} = -\frac{\alpha\beta}{\gamma^3}$$
$$\frac{\partial \cos {}^{t+\Delta t}\theta}{\partial u_{2x}} = -\frac{1}{\gamma}\left(\frac{\alpha^2}{\gamma^2} - 1\right) \qquad \frac{\partial \sin {}^{t+\Delta t}\theta}{\partial u_{2x}} = \frac{\alpha\beta}{\gamma^3}$$
$$\frac{\partial \cos {}^{t+\Delta t}\theta}{\partial u_{1y}} = -\frac{\alpha\beta}{\gamma^3} \qquad \frac{\partial \sin {}^{t+\Delta t}\theta}{\partial u_{1y}} = \frac{1}{\gamma}\left(\frac{\beta^2}{\gamma^2} - 1\right)$$
$$\frac{\partial \cos {}^{t+\Delta t}\theta}{\partial u_{2y}} = \frac{\alpha\beta}{\gamma^3} \qquad \frac{\partial \sin {}^{t+\Delta t}\theta}{\partial u_{2y}} = -\frac{1}{\gamma}\left(\frac{\beta^2}{\gamma^2} - 1\right)$$

for

$$\alpha = ({}^t x_1 - {}^t x_2) + ({}^t u_{1x} - {}^t u_{2x}), \quad \beta = ({}^t y_1 - {}^t y_2) + ({}^t u_{1y} - {}^t u_{2y})$$

where $\gamma = \sqrt{\alpha^2 + \beta^2}$ and $({}^t x_1, {}^t y_1, {}^t z_1)$, $({}^t x_2, {}^t y_2, {}^t z_2)$ are the *global* coordinates for nodes **1** and **2**,

respectively.

4. Results

Results are presented for the benchmark 200-bar and pylon truss structures respectively illustrated in Fig. 2 and Fig. 5: *Non-shape* sensitivity analysis is performed for stress-based functionals in the case of the 200-bar truss; both *shape* and *non-shape* DSA is applied to the pylon structure. Data generated for the sensitivity analyses is verified by comparison with the Finite Difference Method (FDM). This section concludes with a presentation of data generated for the design optimisation of the pylon truss.

4.1. The 200-bar truss

The material and structural characteristics for the 200-bar truss are: Young's modulus $E = 10000$

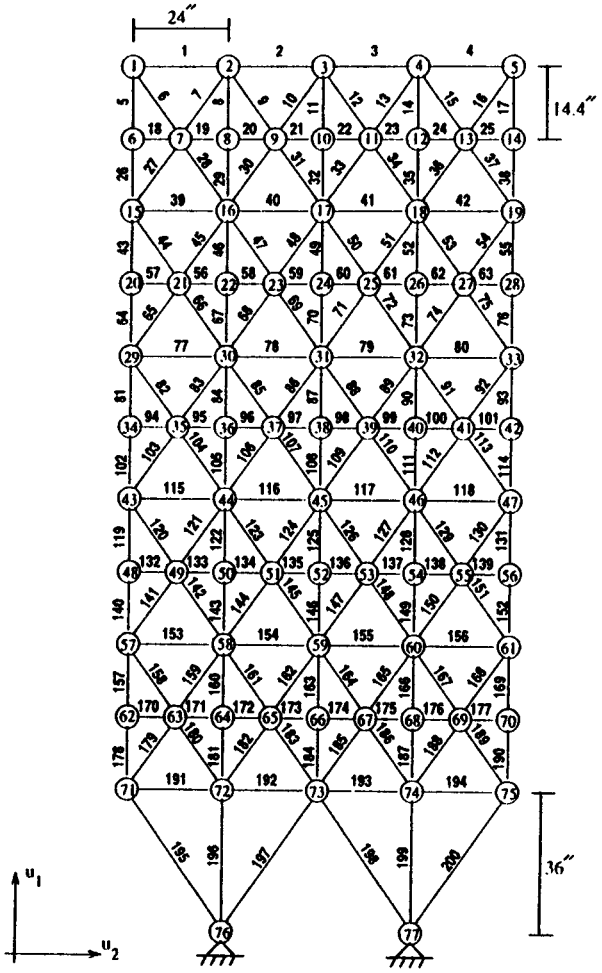

Fig. 2 The 200-bar truss

Table 1 Grouping information for the two-hundred bar truss

Group number	Elements
1	1-4
2	5, 8, 11, 14, 17
3	19-24
4	18, 25, 56, 63, 94, 101, 132, 139, 170, 177
5	26, 29, 32, 35, 38
6	6, 7, 9, 10, 12, 13, 15, 16, 27, 28, 30, 31, 33, 34, 36, 37
7	39-42
8	43, 46, 49, 52, 55
9	57-62
10	64, 67, 70, 73, 76
11	44, 45, 47, 48, 50, 51, 53, 54, 65, 66, 68, 69, 71, 72, 74, 75
12	77-80
13	81, 84, 87, 90, 93
14	95-100
15	102, 105, 108, 111, 114
16	82, 83, 85, 86, 88, 89, 91, 92, 103, 104, 106, 107, 109, 110, 112, 113
17	115-118
18	119, 122, 125, 128, 131
19	133-138
20	140, 143, 146 149, 152
21	120, 121, 123, 124, 126, 127, 129, 130, 141, 142, 144, 145, 147, 148, 150, 151
22	153-156
23	157, 160, 163, 166, 169
24	171-176
25	178, 181, 184, 187, 190
26	158, 159, 161, 162, 164, 165, 167, 168, 179, 180, 182, 183 185, 186, 188, 189
27	191-194
28	195, 197, 198, 200
29	196, 199

ksi; initial bar cross-section $b_i = A = 2.24$ in^2 (for groups[5] i = 1-12, 14, 16, 17, 19, 21, 22, 24, 26), $A = 7.07$ in^2 (i = 13, 15, 18, 20, 23, 25) and $A = 14.14$ in^2 (for i = 27-29}). Applied nodal forces, of uniform magnitude P, act in the positive x-direction at nodes 1, 6, 15, 20, 29, 34, 43, 48, 57, 62, 71, and in the negative y-direction at nodes 1-6, 8, 10, 12, 14-20, 22, 24, ..., 71-75. The functionals $\Psi^{(j)}$ are all of the form $[(\sigma_{11}{}^{(j)}/200)^2 - 1]$, where $j \equiv$element number.

Figs. 3-4 present results for the sensitivity expression (Φ_{199}/b_{200}), for variation in load magnitude P and cross-section b_{200}, respectively.

4.2. The 25-bar pylon truss

The truss constituent material has modulus $E = 6.9 \times 10^7$kPa and the initial bar cross-section $b_i = 3.225 \times 10^{-4}$ m^2 for $i = 1 \ldots 25$. The applied nodal forces, $\boldsymbol{P}^{(3)}$ and $\boldsymbol{P}^{(4)}$, are defined as (1.92, 19.2, $-P_z$) and (-1.92, -19.2, $-P_z$), respectively, where $P_z = 240$ kN. The functionals $\Psi_i^{(j)}$ are all of

[5] Refer to Table 1.

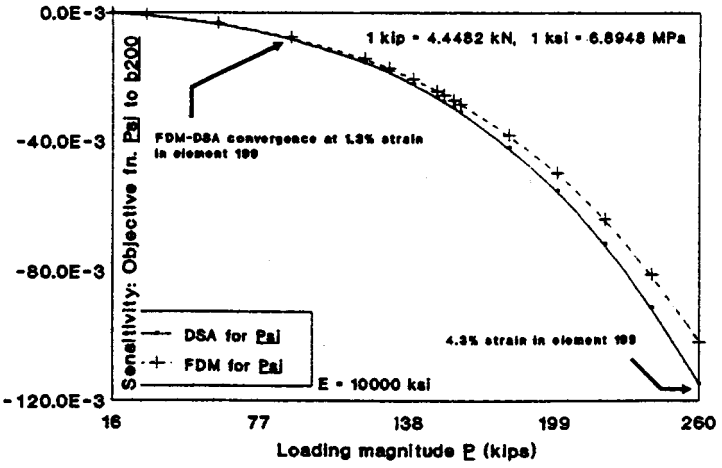

Fig. 3 FDM and DSA sensitivities $\frac{d\Psi_{199}}{db_{200}}$ for variation in P

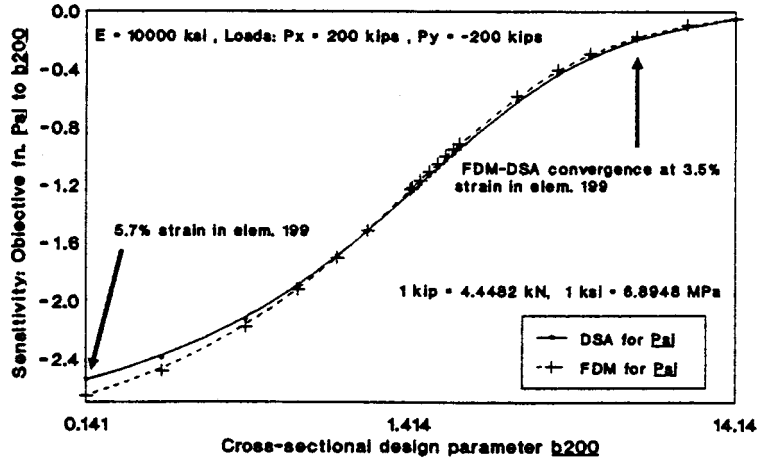

Fig. 4 FDM and DSA sensitivities $\frac{d\Psi_{199}}{db_{200}}$ for variation in b_{200}

the form $[(u_i^{(j)})^2 - 1]$, where $j \equiv$ node number.

4.2.1. Sensitivity analysis of the pylon truss

Fig. 7 tabulates the sensitivity of the displacement-based functional Ψ_z, at node 3, for discrete variations in the pylon structure base area index design parameter h.

Fig. 8 and Fig. 9 present graphical results for the y- and z-displacement functional sensitivities for variation in the *shape* design parameter h and load P_z, respectively.

4.2.2. Structural optimisation of the pylon truss

Structural optimisation of the pylon truss in Fig. 5 is performed for both *shape* and *non-shape*

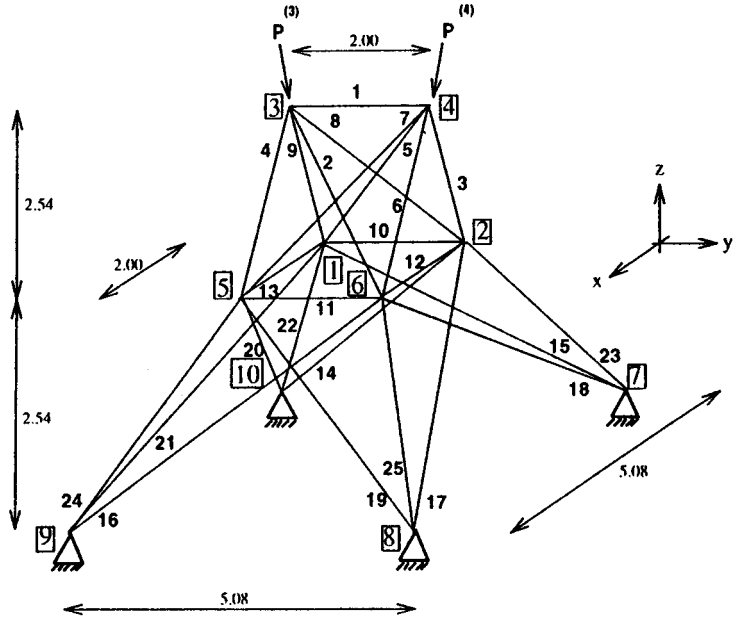

Fig. 5 25-bar pylon configuration

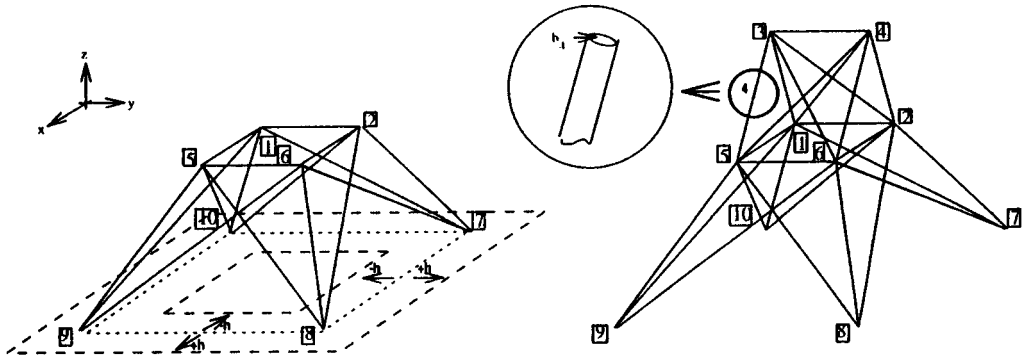

Fig. 6 Shape and non-shape design parameters

design parameters. The design parameters, respectively base area index, h, and the bar cross-sectional area of element **4**, b_4, are graphically defined in Fig. 6.

For the *non-shape* optimisation problem, total material volume is minimised, i.e., $f = \sum_{i=1}^{NEL} L^{(i)} A^{(i)}$ subject to the (side) constraints

$$g_1 = \left(\frac{u_z^{(3)}}{2.5 \times 10^{-2}} \right)^2 - 1 \leq 0, \quad g_2 = \left(\frac{u_y^{(3)}}{2.0 \times 10^{-3}} \right)^2 - 1 \leq 0$$

Table 2 presents the results for the pylon design optimisation, where NI and NF respectively

h	0.00	1.23	2.45
$\frac{d\,\Psi_x^{(3)}}{d\,h}$	0.816E-3	0.377E-2	0.144E-1
b_i=3.225×10^{-4} m^2 with i= ... 25 P_x=240 kN, E=6.9×10^7 kPa			

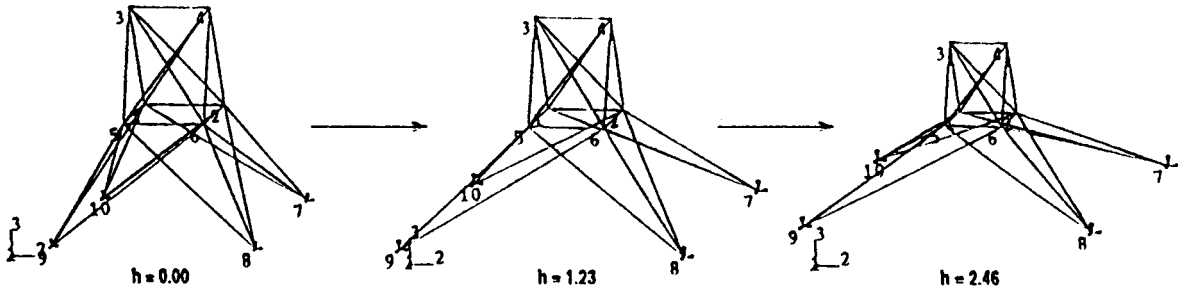

Fig. 7 Structural configuration and *shape* sensitivity $\frac{d\,\Psi_x^{(3)}}{dh}$

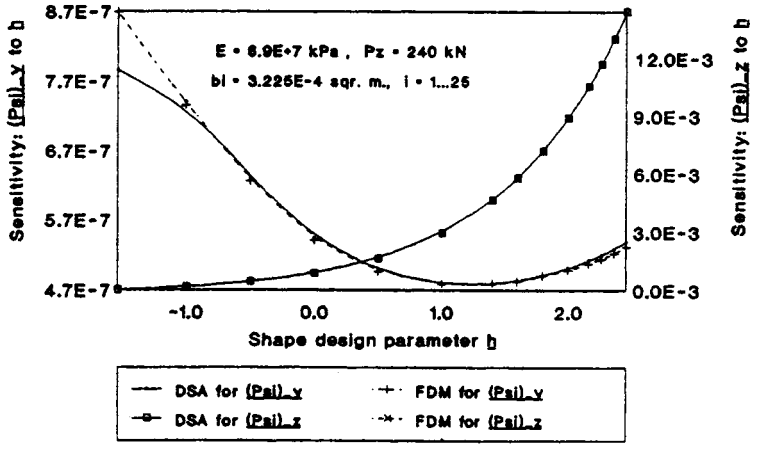

Fig. 8 *Shape* sensitivities $\frac{d\,\Psi_y^{(3)}}{dh}$, $\frac{d\,\Psi_x^{(3)}}{dh}$ vs. design prameter h

represent the total number of iterations and function calls during the optimisation process.

For the *shape* optimisation problem, the objective (cost) function f to be minimized (in the form of a scaled characteristic displacement squared) and displacement constraint g are respectively defined as

$$f = \left(\frac{u_y^{(5)}}{1.0 \times 10^{-4}} \right)^2, \quad g_1 = \left(\frac{u_z^{(3)}}{5.0 \times 10^{-3}} \right)^2 - 1 \leq 0$$

Results for the *shape* optimisation procedure are provided in Table 3.

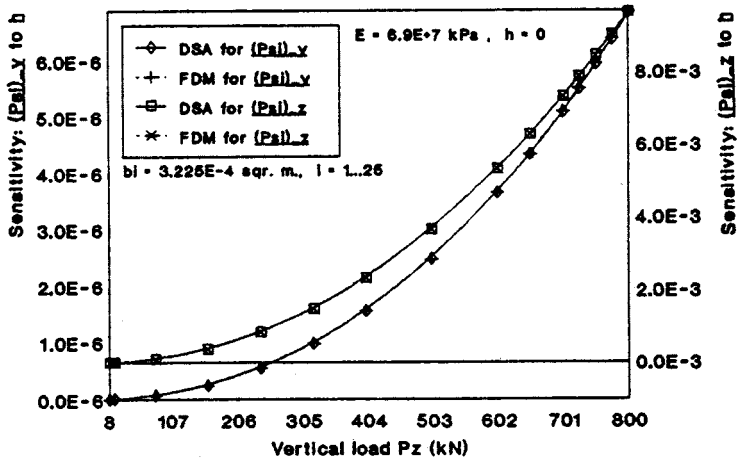

Fig. 9 *Shape* sensitivities $\frac{d\Psi_y^{(3)}}{dh}$, $\frac{d\Psi_z^{(3)}}{dh}$ vs. load P_z

Table 2 Optimising the pylon truss *w.r.t.* cross-section b_4

	Results					
	Initial design	Initial cost	Final design	Final cost	NI	NF
1	1.000×10^{-4} m^2	3.00×10^{-2} m^3	6.239×10^{-3} m^3	4.68×10^{-2} m^3	64	159
2	3.225×10^{-4} m^2	3.06×10^{-2} m^3	5.914×10^{-3} m^3	4.59×10^{-2} m^3	51	127
3	1.000×10^{-3} m^2	3.25×10^{-2} m^3	5.830×10^{-3} m^3	4.56×10^{-2} m^3	27	71

Table 3 Optimising the pylon truss *w.r.t.* base area index h

	Results					
	Initial design	Initial cost	Final design	Final cost	NI	NF
1	-0.025	2.33×10^{-3} m^3	0.482	9.72×10^{-5} m^3	22	39
2	0.000	7.31×10^{-4} m^3	0.493	9.86×10^{-5} m^3	20	33
3	0.025	1.92×10^{-4} m^3	0.485	1.14×10^{-4} m^3	17	26

5. Conclusions

The results presented for the sensitivity analysis and optimisation of the truss structures verify the 'pseudo'-finite element discretisations developed for various categories of sensitivity analysis. The form of these discretisations are sufficiently general to allow for implementation into any established FEA code.

Comparisons between the results produced with these discretisations, the FDM and those arising from DSA formulations involving back substitution of the tangent modulus, underscores the increased accuracy of the DSA formulation outlined in this work, especially in the large strain domain.

The results for sensitivity and optimisation lead to the following conclusions:

- The sensitivity data for the 200-bar truss in Figs. 3-4 underlines the accuracy of the DSA formulation in the large strain domain. Divergence between the FDM and DSA results for large

strain (4%) is attributable to the progressive worsening of the FDM estimates for the increasingly non-linear stress response, combined with the decreased accuracy of the UL kinematic formulation for large strain. For more realistic loading scenarios the close correlation between the DSA and FDM sensitivities are apparent in Figs. 8-9.

- High sensitivity accuracies were obtained for sizeable variations in applied loads, shape and non-shape design parameters. The *shape* sensitivity data, $\partial \Psi_z / \partial h$ vs. h, allows for the most stable base area configuration for the particular loading scenerio to be found by inspection.
- The results for the optimisation of the pylon structure with respect to shape and non-shape design parameters, presented in Tables 2-3, attests to the robustness and efficiency of the PLBA optimisation procedure implementation. A convergence occurs for iteration counts comparable to that reported in the literature for optimal design problems with similar characteristics. The implementation of the PLBA procedure was verified with the benchmark spring problem in Lim and Arora (1986).

References

Arora, J.S. and Cardosa, J.E.B. (1989), "A design sensitivity analysis principle and its implementation into ADINA", *Computers and Structures*, **32**(3/4), 691-705.

Belegundu, A.D. and Arora, J.S. (1985), "A study of mathematical programming methods for structural optimisation-Part 1: Theory", *Int'l Journal for Num. Methods in Eng.*, **21**, 1583-1599.

Bothma, A.S. (1996), "A computational implementation of design sensitivity analysis and structural optimisation", MSc. Thesis, University of Cape Town.

Haririan, M., Cardosa, J.B. and Arora, J.S. (1987), "Use of ADINA for design optimisation of non-linear structures", *Computers and Structures*, **26**(1/2), pp. 123-133.

Kleiber, M., Hien, T.D. and Postek, E. (1994), "Incremental finite element sensitivity analysis for non-linear mechanics applications", *Int'l Journal for Num. Meth. in Eng.*, **37**, 3291-3308.

Kleiber, M. (1993), "Shape and non-shape structural sensitivity analysis for problems with any material and kinematic nonlinearity", *Computer Methods in Applied Mechanics and Eng.*, **108**, 73-97.

Lim, O.K. and Arora, J.S. (1986), "An active set RQP algorithm for engineering design optimisation", *Computer Methods in Applied Mechanics and Engineering*, **57**, 51-65.

Mróz, Z. (1994), "Variational methods in sensitivity and optimal design", *European Journals of Mechanics - A/Solids*, **13**(4-supplement), 115-147.

Thanedar, P.J., Arora, J.S., Tseng, C.H., Lim, O.K. and Park, G.J. (1986), "Performance of some SQP algorithms on structural design problems", *Int'l Journal for Num. Meth. in Eng.*, **23**, 2187-2203.

Tsay, J.J. and Arora, J.S. (1990), "Nonlinear structural design sensitivity analysis for path-dependent problems. Part 1: General theory", *Computer Methods in Applied Mechanics and Eng.*, **81**, 183-208.